Cell and Tissue Research (2023) 392:499–516
https://doi.org/10.1007/s00441-022-03728-4

REGULAR ARTICLE

Biofabrication, biochemical profiling, and in vitro applications of salivary gland decellularized matrices via magnetic bioassembly platforms

Khurshid Ahmed[1] · Teerapat Rodboon[1] · Yamin Oo[1] · Toan Phan[1] · Risa Chaisuparat[1,2] · Supansa Yodmuang[1,3] · Vinicius Rosa[4,5] · Joao N. Ferreira[1]

Received: 25 January 2022 / Accepted: 8 December 2022 / Published online: 28 December 2022

Abstract

Trending three-dimensional tissue engineering platforms developed via biofabrication and bioprinting of exocrine glands are on the rise due to a commitment to organogenesis principles. Nevertheless, a proper extracellular matrix (ECM) microarchitecture to harbor primary cells is yet to be established towards human salivary gland (SG) organogenesis. By using porcine submandibular gland (SMG) biopsies as a proof-of-concept to mimic the human SG, a new decellularized ECM bioassembly platform was developed herein with varying perfusions of sodium dodecyl sulfate (SDS) to limit denaturing events and ensure proper preservation of the native ECM biochemical niche. Porcine SMG biopsies were perfused with 0.01%, 0.1%, and 1% SDS and bio-assembled magnetically in porous polycarbonate track-etched (PCTE) membrane. Double-stranded DNA (dsDNA), cell removal efficiency, and ECM biochemical contents were analyzed. SDS at 0.1% and 1% efficiently removed dsDNA (< 50 ng/mg) and preserved key matrix components (sulfated glycosaminoglycans, collagens, elastin) and the microarchitecture of native SMG ECM. Bio-assembled SMG decellularized ECM (dECM) perfused with 0.1–1% SDS enhanced cell viability, proliferation, expansion confluency rates, and tethering of primary SMG cells during 7 culture days. Perfusion with 1% SDS promoted greater cell proliferation rates while 0.1% SDS supported higher acinar epithelial expression when compared to basement membrane extract and other substrates. Thus, this dECM magnetic bioassembly strategy was effective for decellularization while retaining the original ECM biochemical niche and promoting SMG cell proliferation, expansion, differentiation, and tethering. Altogether, these outcomes pave the way towards the recellularization of this novel SMG dECM in future in vitro and in vivo applications.

Keywords Submandibular gland · Extracellular matrix · Decellularization · Magnetic bioassembly · Cell culture techniques

Introduction

Salivary glands (SG) are exocrine secretory organs that encompass three major pairs of glands in the maxillofacial region and several minor glands lining in the oral mucosa. Altogether, the major and minor salivary glands produce 1–1.5 L of daily saliva (Sui et al. 2020). Saliva is critically important for a better quality of life because it allows for essential functions in the oral cavity and gastrointestinal tract such as digestion, mastication, swallowing, and taste. Upon acinar injury, the function of the water channels that secrete the primary saliva at the epithelial cell surface is reduced, and cells undergo apoptosis. Afterwards, a subjective dry mouth sensation (xerostomia) arises as triggered by the hyposalivation phenomena (Agostini et al. 2018; Sui et al. 2020). Both xerostomia and hyposalivation are

✉ Joao N. Ferreira
Joao.F@chula.ac.th

1 Avatar Biotechnologies for Oral Health and Healthy Longevity Research Unit, Faculty of Dentistry, Chulalongkorn University, Bangkok 10330, Thailand

2 Department of Oral Pathology, Faculty of Dentistry, Chulalongkorn University, Bangkok 10330, Thailand

3 Research Affairs, Faculty of Medicine, Chulalongkorn University, Bangkok 10330, Thailand

4 Faculty of Dentistry, National University of Singapore, Singapore 119085, Singapore

5 Oral Care Health Innovations and Designs Singapore, National University of Singapore, Singapore 119085, Singapore

frequent outcomes of various clinical conditions such as radiotherapy for head and neck cancers, autoimmune conditions (like Sjögren's syndrome), and from side effects of various medications (i.e., diuretics, anticholinergics, antihypertensives) (Miranda-Rius et al. 2015). Currently, available therapies are symptom-based and provide short-term relief only when clusters of secretory acinar epithelial cells remain (Mercadante et al. 2017; Riley et al. 2017).

In vitro biofabrication platforms producing functional SG epithelial organoids as screening tools for novel drugs are of utmost importance to tackle the above common hyposalivation conditions (Tanaka and Mishima 2021). A proper three-dimensional (3D) platform is required to achieve a step-by-step organogenesis process that resembles the development of in vivo glands (Edmondson et al. 2014). Therefore, cell culture systems are crucial to providing SG epithelial cells with an adequate biochemical niche mostly derived from the extracellular matrix (ECM) environment. Moreover, ECMs have been recently investigated to optimize the consistent production of organoids with reproducible morphological shapes through culture, since such organoid biofabrication cannot be achieved with current mouse tumor-derived matrices (i.e., basement membrane extract) (Gilpin and Yang 2017; Aisenbrey and Murphy 2020; Kaur et al. 2021). Ultimately, the presence of tumor-derived ECM components on those SG organoids makes them impossible to reach a clinical trial stage (Chansaenroj et al. 2021). Decellularization of ECM is therefore necessary to offer a biochemical niche for primary and progenitor cells, stem cells, and eventually mature cells to facilitate spatial organization towards an SG epithelial architecture (Mabrouk et al. 2020).

Conventional decellularization strategies involve physical, chemical, and biological removal of cellular and DNA contents while retaining the basic functional biochemical units and molecular cues of the ECM such as heparan sulfate proteoglycans, glycosaminoglycans (GAGs), collagen, and elastin. Various physical, chemical, and biological agents are either applied separately or in combination to decellularize specific tissues (Gilpin and Yang 2017). Common physical decellularization studies include freeze-thawing cycles (Stapleton et al. 2008; Fernández-Pérez and Ahearne 2019), high hydrostatic pressure (Santoso et al. 2014; Hashimoto et al. 2016), and supercritical CO_2 (Casali et al. 2018; Gil-Ramírez et al. 2020). Many physical decellularization methods may require a short duration of treatment at the expense of improper removal of nuclear contents and loss of the ECM biochemical niche (Gilpin and Yang 2017). Chemical-based decellularization has been performed using a perfusion step with various anionic and ionic detergents. Ionic detergents include sodium dodecyl sulfate (SDS) (Lin et al. 2016; Fernández-Pérez and Ahearne 2019; Mayorca-Guiliani et al. 2019) and sodium deoxycholate (Zang et al. 2012; Giobbe et al. 2019), whereas non-ionic detergents include Triton X-100 (Hashimoto et al. 2016; Lin et al. 2016; Elebring et al. 2017), and hypertonic or hypotonic salt solutions (e.g., sodium chloride) (Elebring et al. 2017), or any combination of all of these (Shin et al. 2019). Acids and bases are also applied as chemical agents to decellularize specific tissues and organs. Organic acids such as citric acid, formic acid, acetic acid (Lin et al. 2019; Li et al. 2020), peracetic acid (PAA) (Wolf et al. 2012; Poornejad et al. 2016), and bases (Poornejad et al. 2016; Baptista et al. 2011) have been applied together with the above detergents for organ decellularization. Biological decellularization enzymatic agents can complement such a process (Chen et al. 2004; Ramm et al. 2020; Findeisen et al. 2020). All these reagents and strategies can be performed in multiple combinations; however, the final decellularization approach ultimately requires a complete and efficient breakdown of the leftover DNA residues by an endonuclease (e.g., DNase) for DNA fragmentation into < 200 bp to minimize any potential immunological response.

Decellularization of the submandibular gland (SMG) based on principles from prior methodologies to decellularize human and porcine mammary gland was followed by the development of SMG dECM magnetic-based in vitro high-throughput screening platforms to address the organoid biofabrication challenges related to the lack of consistency and reproducibility using tumor-derived matrices (Ferreira et al. 2021; Maria et al. 2011; Gilpin et al. 2014). We developed the SMG dECM magnetic-based in vitro cell culture platform to evaluate for suitable decellularization for consistent and repeatable organoid biofabrication for future scalability; this methodological approach can be combined with our research team's magnetic bioassembly bioprinting high-throughput platforms and screening assays (Adine et al. 2018; Ferreira et al. 2019; Rodboon et al. 2021; Chansaenroj et al. 2021) as well as for the further characterization of SMG dECM as a suitable bioink for bioprintability. Since porcine SMGs are comparable to their human counterparts, porcine SMG biopsies can be utilized for organoid biofabrication (Urkasemsin et al. 2019). Hence, the aim of this study was to develop porcine SMG dECM using sequential methodological steps combining different concentrations of well-known ionic and nonionic detergents (sodium dodecyl sulfate, triton) and nuclease treatment. To ascertain that biochemical and structural modifications were minimal after decellularization, qualitative and quantitative biochemical and histological characterizations of the SMG dECM were carried out and compared with native ECM. Next, SMG dECM injectable substrate was magnetically bio-assembled on a porous polycarbonate track-etched (PCTE) membrane. This magnetic bio-assembled dECM substrate platform was investigated to determine if such supports primary SMG cell viability, proliferation, expansion, epithelial differentiation, and tethering in vitro. This study hypothesizes that bio-assembled porcine dECM substrates can support primary SMG cell viability, proliferation, expansion, epithelial differentiation, and tethering in vitro.

Materials and methods

Materials

Porcine heads were collected from a commercial local supplier (CP Research and Innovation, Bangkok, Thailand) and disinfected with 70% ethanol. Porcine SMGs were isolated following standard good laboratory practices (GLP) inside a clean room with sterilized 2-mm biopsy punches, forceps, and other surgical equipment. After isolation, glands were collected with a buffer containing HBSS (1 ×), 2% of antibiotic–antimycotic solution (10,000 U/mL of penicillin, 10,000 µg/mL of streptomycin), and bovine serum albumin (30%). Reagents, consumables, and equipment were as follows: Stereomicroscope (SZH10 model, Olympus, Tokyo, Japan), EVOS FL Auto Imaging System (Thermo Fisher Scientific, Waltham, MA, USA), a 2-mm biopsy puncher (Integra Miltex, Plainsboro, New Jersey), phosphate buffer saline (PBS, Vivantis, Malaysia), Triton X-100 (Loba Chemie, India), SDS biological grade (Vivantis, Malaysia, purity 99%), benzonase nuclease (E1014-5KU, Sigma-Aldrich, Merck, St. Louis, MO, USA), Hanks' balanced salt solution (HBSS, Gibco, Thermo Fisher Scientific, Waltham, MA, US), antibiotic–antimycotic solution (containing 10,000 U/mL of penicillin, 10,000 µg/mL of streptomycin, and 25 µg/mL of Amphotericin B, from Gibco). All other reagents were either purchased from Sigma (Merck, St. Louis, MO, US) or Thermo Fisher Scientific (Waltham, MA, US) unless otherwise noted.

Methods

Decellularization of SMG

This experimental study was approved by Chulalongkorn University Faculty of Dentistry Institutional Biosafety Committee (approval numbers DENT CU-IBC 027/2020 and DENT CU-IBC 026/2021). SMG tissue (250 mg) was placed into a sterile Petri dish, and the connective and adipose tissues were removed under a stereomicroscope. Porcine SMG tissue was partitioned with a 2-mm tissue puncher and rinsed with 3 mL of PBS (pH 7.4) 5 times. SMG tissue biopsies were washed in isotonic solutions (PBS) containing sequential concentrations (1–3%) (w/v) of Triton X-100 by using a rocker at 80 rpm for 5 min at room temperature (RT) followed by incubation in 2% (w/v) Triton X-100 for 5 min after each wash. Afterwards, samples were washed in PBS and divided into 3 experimental groups to perform tissue perfusions with different concentrations of SDS, namely, 0.01%, 0.1%, and 1% (w/v) at RT (Supplementary Fig. 1). After such, the SDS solution was cleared from the tissue samples by centrifugation. Decellularized tissues were then washed in PBS containing 2% of the antibiotic–antimycotic solution. Following five thorough washes, tissues were incubated in benzonase nuclease inside an incubator at 37 °C for 18 h. Then, tissue samples were sterilized in 1% of peracetic acid (PAA) for 15 min according to previous protocols (Ferreira et al. 2021) and washed several times with sterile PBS and HBSS containing 2% of the antibiotic–antimycotic solution. SMG dECM biopsy samples (2 mm) were either freshly used for biochemical characterization and cell culture applications or kept at 4 °C or freeze-dried for further investigations (Supplementary Fig. 1).

Quantification of dsDNA

All 2-mm biopsies of native and decellularized freeze-dried SMG tissues were weighed. Tissues were homogenized thoroughly before being transferred to a sterile microcentrifuge tube. Following the manufacturer's instructions, DNA was obtained using Invitrogen's PureLinkTM Genomic DNA Kits (Thermo Fisher Scientific). A Nanodrop ND1000 was used to calculate the amount of DNA in each sample based on absorbance at 260 nm (Thermo Fisher Scientific). More crucially, after this phase, dECM perfused with SDS at 0.1% and 1% (w/v) were chosen for all subsequent studies and investigations because they contained less than 50 ng of dsDNA.

Histochemical analysis

After fixing freshly obtained SMG biopsies and decellularized SMG in 4% paraformaldehyde (PFA), the histochemical examination was done. Specimens were dehydrated in a graded series of alcohols, embedded in paraffin, and then 5-µm-thick sections were prepared. Histological sections were prepared in glass slides for hematoxylin–eosin (HE), mucicarmine, Masson's trichrome, periodic acid—Schiff (PAS), and safranin O staining as recommended by the manufacturer (C.V. Laboratories CO. LTD, Thailand).

BCA protein quantification

A bicinchoninic acid (BCA)™ protein assay kit (Thermo Fisher Scientific) was used to determine the total protein present in the native tissue as well as in SMG dECM. Protein solutions (25 µL) from lyophilized native and decellularized SMG were mixed with 200 µL of BCA working reagent. After 30-min incubation at 37 °C, the absorbance was measured by a microplate reader (GloMax® Discover, Promega, Madison, WI, USA) at 562 nm. A standard curve based on known BSA concentrations (Sigma-Aldrich, Merck) was used as a reference to calculate the protein total amount in each sample.

sGAG biochemical quantification

Sulfated GAG (sGAG) in freeze-dried native SMG tissue biopsies and SMG dECM was measured by using the Blyscan sulfated GAG assay kit (Biocolor Life Sciences, Carrick Fergus, UK) following the manufacturer's instructions. Before quantification, the papain extraction reagent was prepared by adding 400-mg sodium acetate, 200-mg EDTA, disodium salt, and 40-mg cysteine HCl into 50 mL of 0.2 M phosphate buffer (pH 6.4), and finally adding 250 µL of papain suspension into the papain extraction solution. The samples were digested in papain extract solution for 3 h at 65 °C. The concentration of digested sGAG in the experimental sample was measured by using a standard curve prepared from pre-defined sGAG concentrations with the microplate reader (GloMax® Discover) at 656 nm.

Collagen quantification

Freeze-dried SMG biopsies and decellularized SMG ECM were weighed and hydrolyzed in 1 mL of ice-cold 0.5 M acetic acid per 100 mg of the tissue and neutralized to pH 7 with 1 mL of ice-cold 0.5 M NaOH (Truong et al. 2021). The soluble collagen was measured by using a collagen assay kit (Sigma-Aldrich, MAK322) by following the manufacturer's instructions. The collagen concentrations in the experimental groups were measured at fluorescence ʎex = 475/ʎem = 500 nm with the above-mentioned microplate reader (GloMax® Discover). The plotted standard curve of known collagen concentrations was used to determine the total collagen in each experimental group.

Elastin quantification

Elastin contents in freeze-dried SMG and SMG dECM biopsies were measured by the Fastin Elastin Assay (Biocolor Life Sciences, Carrickfergus, UK) by following the manufacturer's instructions. Briefly, the insoluble elastin was converted into α-elastin by incubating in 750 µL oxalic acid (0.25 M) for 60 min at 100 °C. The soluble elastin concentration was measured using an elastin standard curve of pre-defined concentrations. The absorbance of standard and experimental groups was measured at 490 nm using the same microplate reader (GloMax® Discover).

Histological analysis and tissue histomorphometric

HE and Masson's trichrome sections and immunofluorescence micrographs were analyzed with ImageJ software (version 1.8, NIH, Bethesda, US) to quantify nuclear rudiments, collagen distribution, and cellular rudiment removal efficiency. Regions of interest (ROI) from HE and Masson's trichrome sections were manually selected by using threshold intensity in ImageJ. Briefly, the ROI was evaluated using the "Color Threshold" tool. The ROIs were selected by adjusting "HUE" and "Brightness" fields under the Color Threshold tool, and the percent area of ROI was estimated by ImageJ.

Magnetic bioassembly of dECM

SMG dECM suspension was produced in HBSS by crushing the SMG-dECM into micron-size particles for magnetic bioassembly of dECM on porous membranes inside culture plates. To produce a homogenous size distribution, the SMG dECM was filtered with a 40-mesh handy powder sieve. An 18-gauge syringe needle with an inner diameter of 1.2 mm was used to inject the SMG dECM suspension. Following an automated standard concentric release pattern, 20 µL dECM suspension was injected into each well and then the dECM substrate was impregnated on a polycarbonate track-etched (PCTE) porous membrane (Nucleopore Track Etch membrane, Whatman™, Cytiva, Marlborough, MA, USA) at the bottom in 24- and 96-well ultra-low attachment plates. Next, these plates were placed on a magnetic drive with disc-shaped magnetic fields covering the bottom of the wells, and sterilized magnetic pens (Nano 3D Biosciences, Greiner Bio-one, Germany) were inserted on top over the porous PCTE membrane and moved on a standard concentric pattern 3 times to homogeneously distribute the dECM solution for cell culture in vitro applications. For conventional bioassembly via spin coating in the PCTE membrane, the fine matrix suspension was immediately processed as previously reported (Wasnik et al. 2016) with slight modifications. Briefly, 20 µL of SMG dECM was deposited on the PCTE membrane in 24-well culture plates for the goal of expansion under sterile conditions for 10 min at 1200 rpm (Fig. 3a). Then, bio-assembled dECM on PCTE was sterilized with 1% PAA for 15 min and washed five times with 1 × PBS on the orbital shaker at low speed. SMG dECM was then fixed with 4% paraformaldehyde (PFA) for 20 min at an orbital shaker and washed with 1 × PBS three times. Finally, the SMG dECM was incubated with Rhodamine Peanut agglutinin (Rho-PNA, dilution 1:100), washed with 1 × PBS three times, and observed under a fluorescence microscope and scanning electron microscopy (SEM). Using the EVOS FL Auto Imaging System (Thermo Fisher Scientific, Waltham, MA, USA), we were able to measure the thickness of the SMG dECM bioassemblies on PCTE membrane. Briefly, z-stack images were taken at 20 × magnification within a 5-µm interval. Individual SMG-dECM bioassemblies were identified based on Rho-PNA distribution, and their thickness was quantified on conventional and magnetic bioassembly substrate platforms by measuring the thickness of the Rho-PNA labeling using ImageJ.

Scanning electron microscopy

Fresh 2-mm SMG dECM biopsies were used to determine the microarchitecture, structure, and fibril organization and distribution of the dECM (before magnetic bioassembly and cell culture), whereas the microarchitecture and fibril organization of the SMG dECM magnetic bioassembly PCTE substrates (before cell culture) were studied using the previously prepared SMG dECM magnetic bioassembly. To study primary SMG cell tethering and proliferation on SMG dECM magnetic bioassembly PCTE substrates, after 7 cell culture days, SMG dECM magnetic bioassembly PCTE substrates was investigated and compared to SMG tissue biopsies on PCTE membrane. All samples were fixed with 2.5% glutaraldehyde for 40 min and were dehydrated by using a series of alcohol concentrations (from 40 to 100%) and dried in a Critical Point Drier (Quorum K850, Lewes, East Sussex, UK). Then, specimens were fixed with 1% osmium tetroxide in 1 × PBS solution for 30 min at RT, coated with gold, and observed under a scanning electron microscope or SEM (FEI Quanta 250 FEG, Thermo Fisher Scientific).

SMG cell viability, proliferation, expansion, tethering assays, and phenotypic characterization

Porcine primary SMG cells were mechanically and enzymatically extracted and isolated following previous protocols (Pringle et al. 2011; Rodboon et al. 2021). Next, cell viability and proliferation assays were conducted by seeding porcine primary SMG cells on the magnetic bioassembled SMG dECM (previously perfused with 0.1% and 1% SDS). Briefly, this magnetic-formed dECM was placed in ultra-low attachment 96-well plates, seeded with 2×10^3 cells/well, and incubated at 37 °C and 5% CO_2 for 30 min to let cells settle on the dECM substrates. After 30 min, wells were supplemented with growth media comprising Dulbecco's modified Eagle medium (DMEM)/F12 (Gibco, Thermo Fisher Scientific) containing 10% FBS and 1–10% of a solution with antibiotics and an anti-mycotic as per previous protocols. This media was replaced every 2 days. Cell viability and proliferation were evaluated for 7 days by using ReadyProbes™ cell viability imaging kit (Molecular Probes, Thermo Fisher Scientific), MTT (3-[4,5-dimethylthiazol-2-yl]-2,5 diphenyl tetrazolium bromide) assay, and CellTiter-Glo® (Promega, Madison, WI, USA) at baseline (after 2 h of culture), day 3, day 5, and day 7. Basement membrane extract (BME, Cultrex™, R&D systems, Minneapolis, MN, US) substrates and plastic surfaces in 96-well plates were used as positive and negative controls, respectively, to compare with the SMG dECM magnetic bioassembly platforms. The absorbance (for MTT) and luminescence (for CellTiter-Glo®) were measured using a microplate reader (GloMax® Discover) following manufacturer instructions.

Cell expansion was assessed by calculating SMG primary cell confluency rates at pre-defined proliferation time points (baseline, days 3, 5, and 7) using ImageJ software (NIH).

To analyze cell tethering before and after recellularization, SMG dECM magnetic bioassembly PCTE specimens and control SMG tissue biopsies on PCTE membrane were fixed in 2.5% glutaraldehyde for 40 min for SEM. As mentioned above, SEM samples were dehydrated, dried, fixed with 1% osmium tetroxide, coated with gold, and observed under the previous SEM (FEI Quanta 250 FEG).

After being fixed for 30 min at RT in 4% paraformaldehyde, cells were washed multiple times in PBS, permeabilized for 10 min in 0.1% Triton X-100 (Sigma-Aldrich), and then blocked in 5% BSA and 10% horse serum overnight at 4 °C. Primary antibodies were incubated at 4 °C overnight with 0.1% Triton X-100 for Ki67 (catalog no. SK2482872, Invitrogen), Aquaporin-5 (AQP5, catalog no. ab92320, Abcam), Cytokeratin 19 (K19, catalog no. ab181595, Abcam), and α-smooth muscle actin (α-SMA, catalog no. ab5694, Abcam). Samples were then treated with one of the following secondary antibodies for 2 h at RT: Alexa Fluor 488 goat anti-rabbit IgG (catalog no. ab150077, Abcam) or Alexa Fluor 594 goat anti-rabbit IgG (catalog no. ab150080, Abcam), each at a dilution of 1:200. Staining of nuclei was done with Hoechst 33,342 (Life Technologies, Thermo Fisher Scientific).

Statistical analysis

Data are always displayed as means ± standard deviations (SD). One- and two-way ANOVA followed by *Tukey* post hoc tests were performed to compare three or more experimental groups. All statistical analyses were performed using Prism version 9 (GraphPad Software, Inc., San Diego, CA, USA).

Results

Decellularization is a suitable strategy towards the development of organ biofabrication platforms for in vitro SG investigations and cell screening assays. Nevertheless, reproducible decellularization requires screening platforms to ensure cell viability, proliferation, consistent expansion, and cell tethering mechanisms. First, we established herein a new decellularized SG platform to clear all immunogenic DNA components while retaining the important ECM biochemical niche from the native SG. To meet this purpose, SMG biopsies were first perfused with varying SDS concentrations (0.01%, 0.1%, and 1%) and treated with endonuclease thereafter.

dsDNA and nuclear removal efficiency was established with 0.1% and 1% SDS perfusions

Firstly, the visual appearance of the SMG ECM changed as expected under an initial stereomicroscope analysis (Supplementary Fig. 2). Decellularization efficiency was investigated based on cellular and DNA/nuclear cleansing as well as the retention of the important biochemical cues located in the native ECM.

To prevent future potential immune responses, the developed dECM must contain dsDNA less than 50 ng/mg dry weight by standard guidelines (Crapo et al. 2011). In this study, the quantification of dsDNA confirmed that SMG biopsies perfused with 0.1% and 1% SDS removed most of the dsDNA by bringing these nuclear contents below the cut-off value of 50 ng/mg dry weight (Fig. 1a). Furthermore, it was observed that 0.01% SDS-treated dECM still contained dsDNA debris higher than the cut-off as well as greater nuclear contents and rudiments (Fig. 1a–g). More than 95% of cellular debris removal was observed after SMG biopsies were perfused with SDS (Fig. 1c), and such removal improved with increasing concentrations of SDS (95% for 0.01% SDS vs. 99% for 1% SDS; Fig. 1c).

Next, SMG dECM and native SMG tissue biopsies were stained with Rho-PNA (fluorophore-conjugated). Peanut agglutinin is a galactose-specific lectin that stains Gal-β(1,3)-GalNAc of mucosubstances including mucins and other glycoproteins as well (Carvalho et al. 2018; Kim et al. 2009). Mucosubstance-specific Rho-PNA dye, mucicarmine staining, and hematoxylin–eosin (HE) were investigated to understand the effect of SDS on the glandular mucins and nuclear components. Rho-PNA micrographs exhibited a prominent decrease in mucins with 1% SDS perfusion (Fig. 1d−g), The densely distributed mucin layers seen in native SMG were partially removed and loosely dispersed by SDS in SMG dECM. As expected, 1% SDS had a higher rate of removal and dispersion when compared to 0.1% SDS (Fig. 1f, g; Supplementary Fig. 3). HE sections stained pinkish-purple structures confirming the presence of eosinophilic collagen on the native SMG tissues (Fig. 1d'−g'; Supplementary Fig. 3), whereas in the SMG dECM, no basophilic staining was observed (typically seen when nuclear contents are present), except in the ones perfused with 0.01% SDS (where dark blue nuclei were present; Fig. 1e''; Supplementary Fig. 3). Therefore, from here onwards, SMG-derived dECMs developed with 0.1% and 1% of SDS perfusion were selected for further investigations and to manufacture the magnetic bioassembly platform for in vitro cell culture applications.

Retention of native ECM proteins and sulfated proteoglycans

The preservation of important ECM biochemical niche components was determined with quantitative biochemical assays and histomorphometric analysis. In this study, the developed dECM could maintain 96% of sulfated glycosaminoglycans (sGAG) when compared to native ECM (Fig. 2a). sGAGs are well-known important components of the SG basement membrane (Patel et al. 2017). Moreover, dECM with 0.1% SDS perfusion treatment could preserve collagens (~60.3%) ($p < 0.001$; Fig. 2b). Next, SMG dECM (with 0.1% or 1% of SDS perfusion treatments) and native SMG tissue biopsies were stained with mucicarmine and Masson's trichrome to understand the effect of SDS on the retention and distribution of ECM biochemical niche components. Histological sections stained with mucicarmine showed a distribution of mucins (deep rose color appearance) across the native tissue which was present in the native SMG ECM and SMG dECM specimens (Supplementary Fig. 3). The blue staining in Masson's trichrome sections confirmed the presence of collagen distribution in the SMG dECM developed with 0.1% and 1% SDS as observed earlier by Agarwal et al. (2018) (Fig. 2c−e). Safranin-O stain for mucosubstances such as GAG (red is a positive stain) also demonstrated clear retention of this mucosubstance (Fig. 2c'−e'). Additionally, PAS, which stains the glycoproteins magenta, exhibited retention of glycoproteins in the SMG dECM.

Moreover, dECM with 0.1% SDS perfusion treatment maintained elastin (~78.2%), and this was achieved to a significantly lesser extent with 1% SDS ($p < 0.001$; Fig. 2f). Protein quantification after BCA assay confirmed that total protein decreased 3-fold with 0.1% SDS and about 10-fold with 1% SDS ($p < 0.0001$; Fig. 2g). Furthermore, histological specimens and quantification with ImageJ revealed that collagen fibers were more evenly distributed across the dECM compared to native SMG tissue specimens ($p < 0.0001$; Fig. 2c'−e', h). However, the SMG dECM perfused with 1% SDS showed a higher percentage of collagen distribution on its surface (Fig. 2h) indicating that SDS had loosened the ECM integrity and thus facilitated the distribution of the displaced matrix components including collagens as per previous reports (Haupt et al. 2018).

Table 1 Primary SMG cell confluency on different substrates and platforms including BME, SMG dECM developed with 0.1% and 1% SDS perfusions. ImageJ software was used to calculate the confluency rate for $n = 10$. Values are displayed as means ± SD

Expansion confluency rates (%)				
Substrates/platforms	Baseline	3-day	5-day	7-day
BME	8.2 ± 1.4	10.6 ± 1	22.74 ± 3.2	56 ± 4.0
SMG dECM 0.1% SDS	8.2 ± 2.4	11.3 ± 3.2	27 ± 2.8	58.2 ± 6.3
SMG dECM 1% SDS	9 ± 1.5	19 ± 4.2	30 ± 5.0	68 ± 5.7

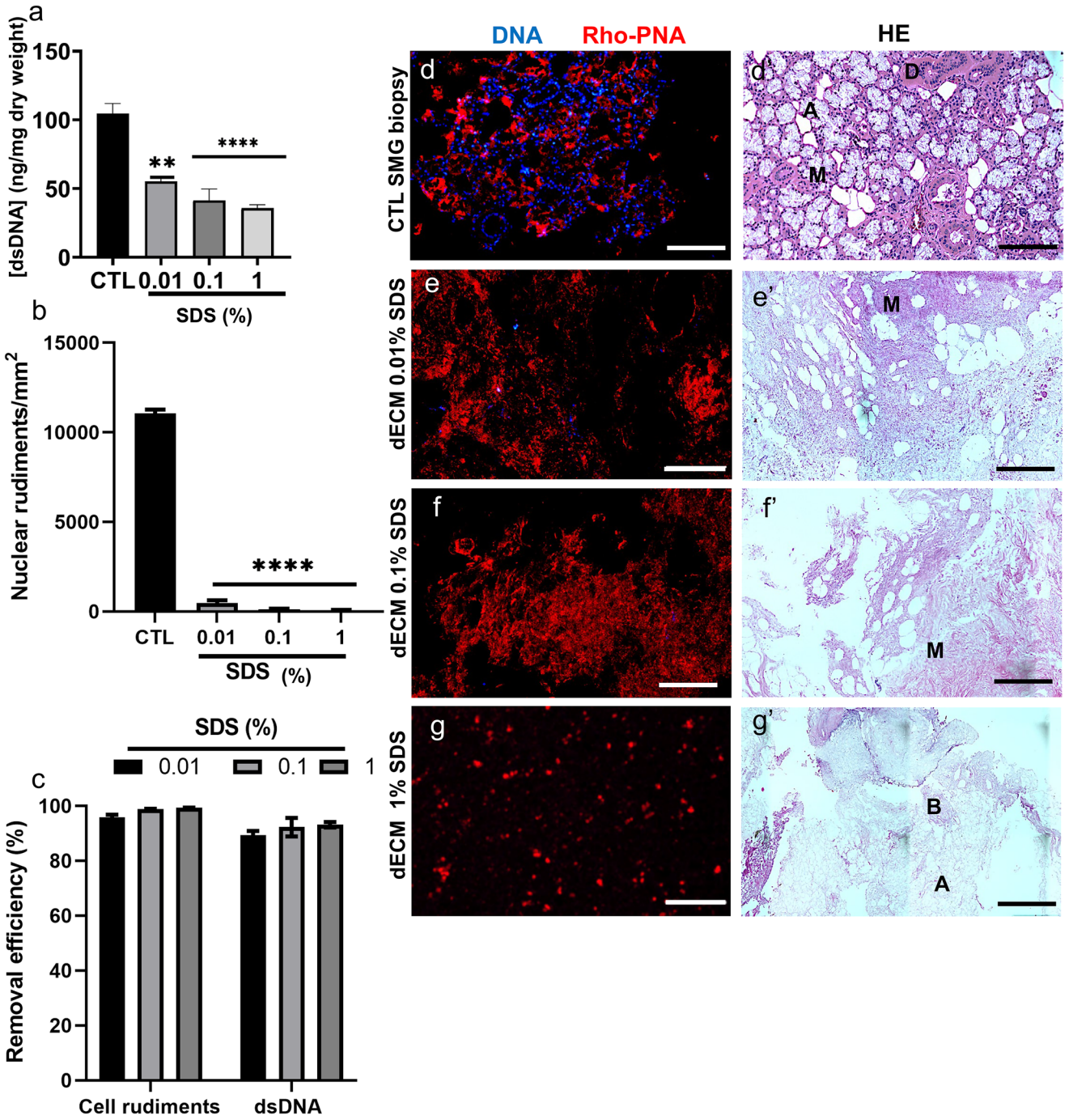

Fig. 1 SDS treatment of SMG ECM at 0.1% and 1% removed nuclear contents to a level lower than 50 ng dsDNA after SMG decellularization and preserved basement membrane mucins. **a** Quantification of dsDNA after SMG decellularization and varying SDS perfusion treatments (0.01%, 0.1%, and 1%). **b** Quantification of nuclear rudiments after decellularization with varying SDS treatments. **c** Cell removal efficiency after varying SDS treatments. All column bars represent the mean values and error bars SD for $n = 4–7$. $^{**}p < 0.001$; $^{****}p < 0.0001$ when compared to CTL (control native tissue biopsies) by one-way ANOVA with Tukey post hoc test. **d–g** Removal of nuclear contents (Hoechst 33,342 blue fluorescence staining) and preservation of basement membrane mucins (Rho-PNA red fluorescence staining dye) in SMG dECM developed with 0.1 and 1% SDS showed mucins across the dECM (5 µm thick section with 20–50 mm^2 area) but absence of nuclear rudiments. Incomplete decellularization of tissue sections with 0.01% SDS still displayed a few nuclear contents, whereas **d'–g'** hematoxylin–eosin (HE) stitched sections showed acini (A), duct (D), and mucin (M) before and after decellularization. Magnification (Mag.): 20×. Scale bar: 50 µm

Decellularized matrix microarchitecture and ultrastructure were comparable to the native ECM

SMG dECM specimens were then analyzed in terms of microarchitecture and ultrastructure integrity. SEM micrographs displayed a removal of epithelial sheets after decellularization while retaining the fine fibrillar arrangements of ECM structural components (Fig. 2c"–e"; Supplementary Fig. 4). Interestingly, the 3D voids in dECM microarchitecture created by the removal of various cells remained intact. At higher magnification, the ECM structure appeared unscathed, and the direction of dECM fibers like collagen also remained intact (Figs. 2c"–e" and 4).

Cell proliferation, expansion, tethering, and differentiation were present in SMG dECM bioassembly platforms

Next, we designed a new biofabrication strategy that used a magnetic bioassembly platform against commercial porous PCTE for future in vitro 2D/3D organoid screening assays and recellularization applications (Fig. 3a). Magnetic forces (established and driven by magnetic drives and pens) were used to flatten the freshly dECM on porous PCTE membranes. The dECM thickness was analyzed and measured by staining with Rho-PNA (since dECM was earlier found to be 90% rich in mucosubstances including sGAGs; Figs. 1 and 2; Supplementary Fig. 3). Under fluorescence microscopy, dECM thickness was on average 15.41 µm (±0.64) (Fig. 3b) with a very narrow variation that reassured the consistency of the SMG-dECM bio-assembled by magnetic forces. Conversely, the conventional spin-coated dECM platforms greatly varied in thickness (46.52 µm ± 18.78), and thus, such was not deemed consistent and reproducible (Fig. 3b, c, c'). Additionally, both bio-assembled platforms, the spin-coated and the magnetic bio-assembled SMG dECM, were also investigated under the SEM to evaluate the microarchitecture integrity, whereas a tenfold increase in the SDS perfusion resulted in a finer fibrillar network of dECM (Figs. 3d, d' and 4).

Primary SMG cells were then seeded on the SMG dECM magnetic bio-assembled platforms as well as on conventional BME substrates, representing commercially standard positive controls for cell and organoid proliferation and expansion. Primary SMG cells' responses to different substrates were investigated by standard MTT biochemical assays (Fig. 5a) and CellTiter-Glo® luciferase assays (Supplementary Fig. 4a, b). Bio-assembled SMG dECM perfused with 1% SDS showed a greater MTT-based proliferation rate than BME at day 3 ($p < 0.0001$; Fig. 5a) and at day 5 with both 0.1% and 1% SDS ($p < 0.001$ and $p < 0.0001$, respectively; Fig. 5a). Expression of Ki67 pro-mitotic marker supported these findings after immunocytochemistry (Fig. 5b–d'). Primary SMG cells consistently had on average a 2-fold higher proliferation through culture (at days 3, 5, and 7) on SMG dECM perfused with 1% SDS as compared with commercial BME controls. Comparable findings were observed with CellTiter-Glo® luciferase-based assays on both dECM and BME (Supplementary Fig. 4a). In plastic surface plates, the MTT proliferation rate was slower with the same seeding density as the other cell culture dECM platforms (Supplementary Fig. 4b).

Next, protein expression levels of SMG epithelial markers were investigated, including AQP5 (acinar), K19 (ductal), and α-SMA (myoepithelial), as well as Ki67 for pro-mitotic cells. When compared to the baseline, bio-assembled SMG dECM perfused with 0.1% promoted APQ5 expression ($p < 0.0001$) (Fig. 6a). When comparing to commercially available BME and plastic surfaces, SMG dECM magnetic bioassemblies produced by 0.1% and 1% SDS perfusion increased the expression of APQ5 and K19 (Fig. 6b–d"; Supplementary Fig. 7), but such differences were not significant. Phenotypic expression of α-SMA was unchanged relative to baseline in all substrates and controls (Fig. 6; Supplementary Fig. 7). As expected, while cell confluency and epithelial differentiation takes place, cell renewal and mitosis decreases, as observed with the expression levels of Ki67, which is significantly reduced from baseline to 7 days (Figs. 5b and 6a). Additionally, SMG dECM perfused with 0.1% and 1% SDS exhibited comparable expression patterns for ductal and myoepithelial markers when compared to BME (Fig. 6a; Supplementary Fig. 7) and plastic culture surface (Supplementary Fig. 8).

Primary SMG cells were also tracked with Hoechst 33,342 (Life Technologies, Thermo Fisher Scientific) to investigate cell confluency rates and cell tethering capacity of our bio-assembled SMG dECM platforms. SMG dECM perfused with 1% SDS provided better cell confluency rates

Fig. 2 After decellularization with 0.1% and 1% SDS perfusion treatments, retention of ECM biochemical components was established. **a** Sulfated GAG (sGAG) and **b** total collagen quantification in control SMG tissue samples (CTL) and decellularized matrices. **c–e** Safranin O staining of the SMG dECM revealed a red hue indicative of GAG (G) presence. **c'–e'** Masson's trichrome was used to create a blue stain on the collagen contents (C) of the SMG (right micrograph panel). Where A represents acini and D represents duct. Whereas a similar pattern can be seen in Masson's trichrome as well as in **c"–e"** SEM micrographs of SMG dECM perfused with 0.1% and 1% SDS. Mag.: 60×. Scale bar: 50 µm, SEM: Mag.: 20,000×. SEM: Scale bar: 50 4 µm. **f** Biochemical quantification of elastin from dECM and CTL SMG tissues. **g** Quantification of total protein from dECM and CTL. **h** Distribution of collagen fibers in dECM and CTL SMG from Masson's trichrome sections. Micrographs and quantification are based on 5-µm-thick sections with a 20–50 mm^2 area. Error bars represent SD from $n = 4–10$. ***$p < 0.001$, ****$p < 0.0001$. dECMs were compared to CTL by one-way ANOVA analysis with Tukey post hoc test

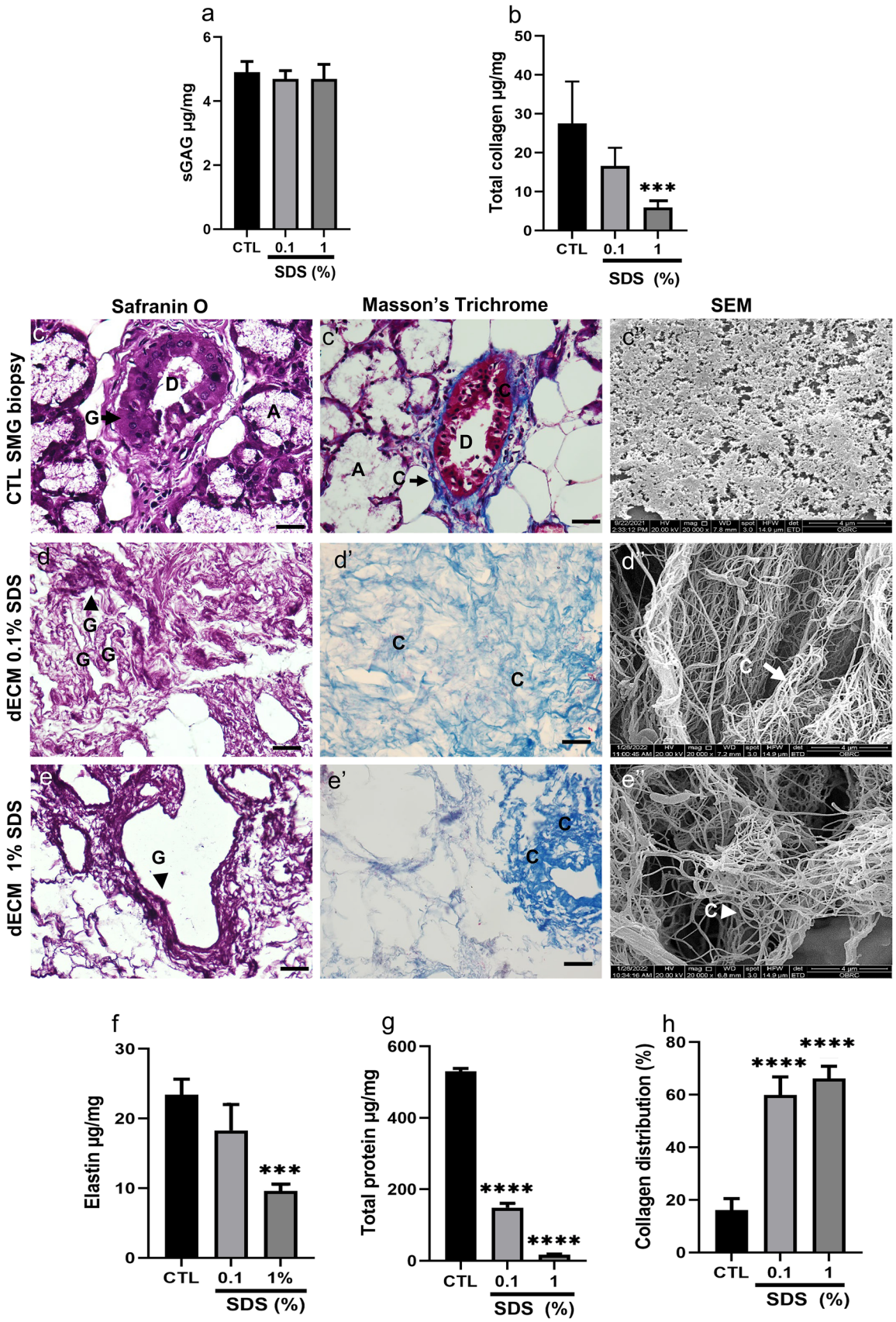
a
sGAG µg/mg
CTL
0.1
1
SDS (%)
b
Total collagen µg/mg
***
CTL
0.1
1
SDS (%)
Safranin O
Masson's Trichrome
SEM
CTL SMG biopsy
dECM 0.1% SDS
dECM 1% SDS
c
c'
c''
d
d'
d''
e
e'
e''
D
G
A
C
f
Elastin µg/mg
***
CTL
0.1
1%
SDS (%)
g
Total protein µg/mg
****
****
CTL
0.1
1
SDS (%)
h
Collagen distribution (%)
****
****
CTL
0.1
1
SDS (%)

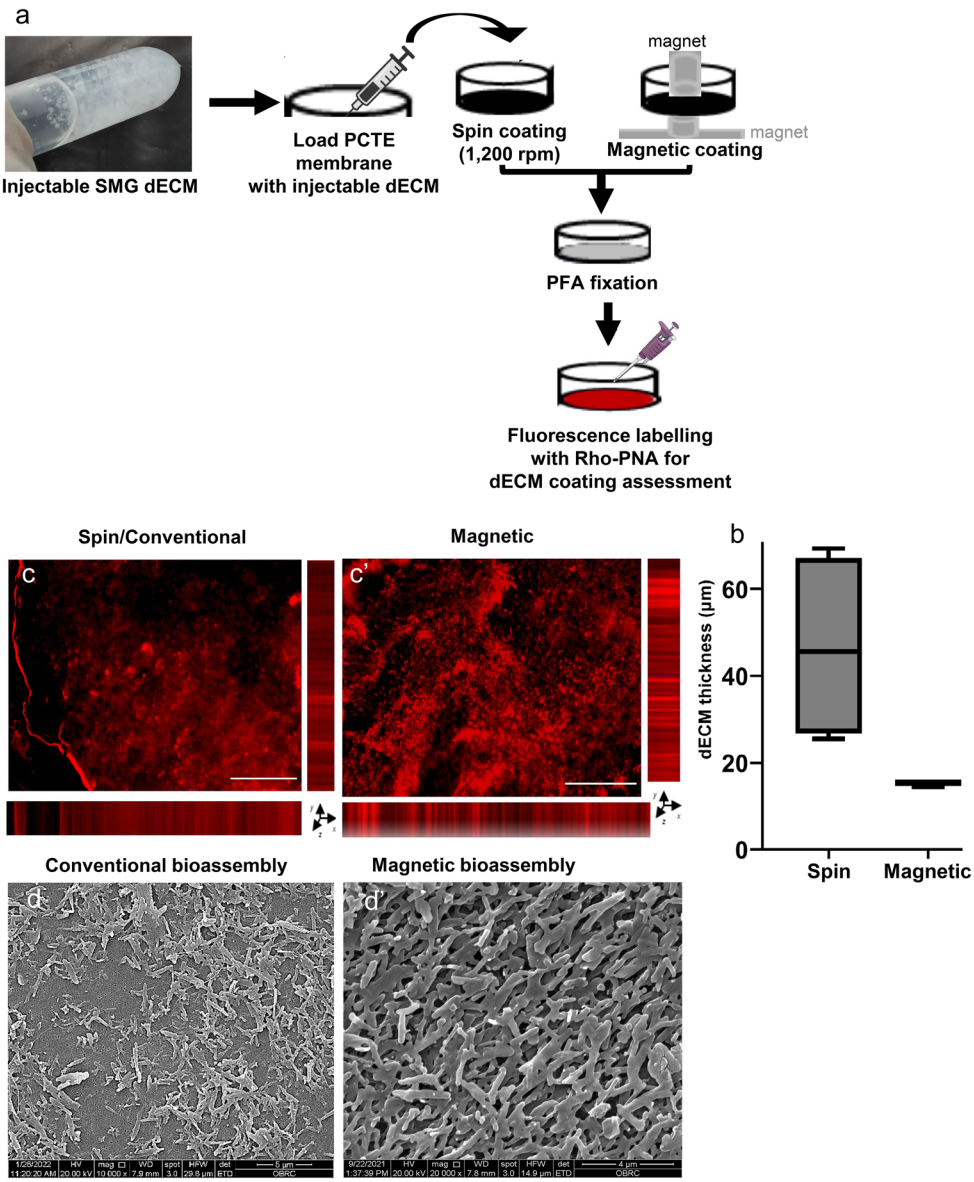

Fig. 3 Magnetic bioassembly platforms on PCTE produced dECM coatings more evenly and consistently when compared to spin coating conventional methods. **a** Methodological strategies for coating SMG dECM on PCTE (polycarbonate track-etch) porous membranes followed by fixation with 4% paraformaldehyde (PFA) and tagging with Rho-PNA for coating assessment to determine dECM distribution and thickness on PCTE. Created with BioRender.com. **b** dECM substrate thickness on conventional and magnetic bioassembly platforms on PCTE. **c–c'** Distribution of ECM substrates on PCTE on conventional and magnetic bioassembly platforms after Rho-PNA labeling. Mag.: 20×. Scale bar: 50 µm. **d–d'** SEM micrographs of conventional and magnetic bioassembly of SMG dECM substrates on PCTE. Mag.: 20,000×

(68% for SDS 1%, 58.2% for 0.1% SDS, and 56% for BME) and cell tethering, which was followed by SMG dECM with 0.1% SDS (Supplementary Fig. 5 and Table 1). In addition, the potential of SMG dECM for cell tethering was also analyzed by SEM on day 7 in in vitro cell culture applications. A clear sheet of epithelial cells was engrafted on SMG dECM bioassembly PCTE substrate, which was particularly prominent in the ones perfused with 1% SDS (Fig. 7).

In summary, the magnetic bio-assembled SMG dECM substrate platforms perfused with 0.1–1% SDS promoted SMG primary cell proliferation, expansion confluency rates, ductal epithelial differentiation, and tethering. The dECM perfused with 0.1% SDS tend to promote great acinar epithelial differentiation when compared with other substrates and conventional organoid substrates like BME, while the ones perfused with the 1% SDS supported a higher cell proliferation rate from 3 culture days onwards.

Discussion

Herein, the establishment of a novel in vitro dECM-based SG biomaterial scaffold after perfusion with 0.1% and 1% SDS, an ionic detergent combined with a commercial endonuclease, was successfully cleared from dsDNA and nuclear contents as recommended elsewhere (Crapo et al. 2011; Gilpin and Yang 2017). This occurred while preserving

most of the native SMG ECM biochemical niche, its histology and microarchitecture. Moreover, after perfusion with 0.1% and 1% SDS, this dECM biomaterial upon magnetic bioassembly inside a regular well plate achieved a consistent thickness, microarchitecture, and fibrillar ultrastructure in the final in vitro 2D/3D cell culture platform. This final dECM platform exhibited a greater cell proliferation, confluency expansion, and tethering when compared with conventional substrates, particularly the ones perfused with 1% SDS (Figs. 5, 6, and 7, and Supplementary Figs. 4, 5, 6, and 7). Furthermore, perfusion with 0.1% SDS enhanced acinar and ductal epithelial differentiation, while the 0.1% SDS and all other substrates tend to support only ductal epithelial differentiation after 7 days. Myoepithelial cell populations remain stable through culture.

Currently available therapeutics to treat dry mouth mainly consider easing the symptoms or reestablishing a residual glandular function (Furness et al. 2013; Mercadante et al. 2017; Riley et al. 2017; Ferraiolo and Veitz-Keenan 2018). Nevertheless, our research group's discovery of in vitro bioprinting platforms to facilitate SG organoid formation and screening was important to provide more suitable high-throughput platforms rather than in vivo animal experimentation (Adine et al. 2018; Ferreira et al. 2019; Nie et al. 2020; Tanaka and Mishima 2020; Chansaenroj et al. 2021). This is an essential step for other exocrine glands like lacrimal and mammary glands in healthy and pathological conditions (Rijal et al. 2018; Rodboon et al 2021; Ferreira et al. 2021; Nerger and Nelson 2019). However, in vitro organogenesis requires matrix morphogenesis and thus biomaterial scaffolds that provide a biochemical niche and microarchitecture leading towards cell tethering, growth, and maturation (Chung et al. 2020). Various biomaterials such as hyaluronic acid (Lee et al. 2020) and alginate hydrogel microtubes (Jorgensen et al. 2022) have been tested in ex vivo SMG organogenesis. However, dECM continues to be the most fitting biomaterial because it does not only offer microarchitectural support to primary or stem cells but also cell tethering if the decellularization process can maintain the biochemical, histological, and microarchitecture features (Frantz et al. 2010; Patel et al. 2017, 2021; Clara et al. 2018).

In our decellularization strategy, perfusion with 0.1% and 1% SDS efficiently removed dsDNA (below 50 ng/mL), maintained mucins and sGAG, but lost large protein molecules such as collagen and elastin by about 10-fold or less, with SDS 1% and 0.1%, respectively (Fig. 2). Comparable outcomes were achieved with dECM from rat SG but with SDS 10% perfusion for 32 h (longer time when compared to the 50 min required for our dECM methodology); however, researchers did not assess sGAG content (Gao et al. (2015). Later, Shin et al. (2019) also applied 1% SDS to decellularize rat SMG for about 18 h (longer perfusion compared to our strategy as well) and unlike previous reports (Gao et al. 2015), researchers evaluated sGAG along with the basic structural proteins. sGAGs are important for glandular epithelium since human lung decellularization can result in a significant loss of sGAG or the GAG disaccharide composition, leading to malfunctions in the decellularized glands (Uhl et al. 2020). The depletion of sGAG and tissue-specific growth factors would certainly influence the recellularization process (Elebring et al. 2017). Interestingly, sGAG contents in the glandular epithelium of the exocrine pancreas were investigated after a decellularization strategy with a cocktail of 4% (w/v) sodium deoxycholate and 6% (v/v) Triton X-100 for 8 h (Elebring et al. 2017). Unlike our protocol, this decellularized strategy in the pancreas ECM could only retain 50% of sGAG. Hashemi et al. (2018) reduced the Triton X-100 perfusion to 0.25%, and after 12-h perfusion with Triton X-100 combined with 6-h perfusion with 0.5% SDS, this group was able to retain more sGAG, approximately 60%, but still lower than 96% achieved with the biochemical investigations to our dECM. Additionally, a prolonged SDS exposure via perfusion can not only damage the ECM biochemical niche and proteoglycan components but would leave in the ECM leftover SDS debris that could be cytotoxic for in vitro cell and tissue culture applications (White et al. 2017). The dECM scaffold produced herein, besides containing a smaller amount of fibrillar proteins such as collagen and elastin (10-fold or less than the native SMG), was still able to maintain mucins and sGAG components in the biochemical niche. SGAGs are proteoglycans that play important functions in SG morphogenesis, growth factor regulation, and basement membrane integrity (Patel et al. 2017). Whereas mucins are relevant for cell–cell and cell-ECM interactions and are a reservoir for bioactive materials such as large proteins and peptides responsible for bioavailability and bioactivity of signaling cues (Petrou and Crouzier 2018). In our study, consistent distribution of mucins across the SMG dECM can anticipate the presence of naturally occurring growth factor cues or cytokines that are usually bounded to mucins (Choi et al. 2012). For instance, bio-engineered SG developed by seeding salivary epithelial clusters in tumor-derived matrices such as BME and/or Matrigel revealed a greater phenotypic expression of acinar cells in the presence of fibroblast growth factor 2 (Hosseini et al. 2018). This indicates sequestered signaling cues are vital for cell–cell and cell-ECM interactions and ex vivo morphogenesis (Patel et al. 2017, 2021). Various ECM proteins including collagen, fibronectin, and laminin have also been investigated as cell culture substrates but individually; nonetheless, each one of them can play a relevant role in tuning phenotypic and physiological activities (Nam et al. 2017; Lee et al. 2014; Carlsson et al. 1981; Choi and Choi 2013).

Interestingly, primary SMG cells tracked with nuclear dyes and two standard proliferation assays inside the in vitro

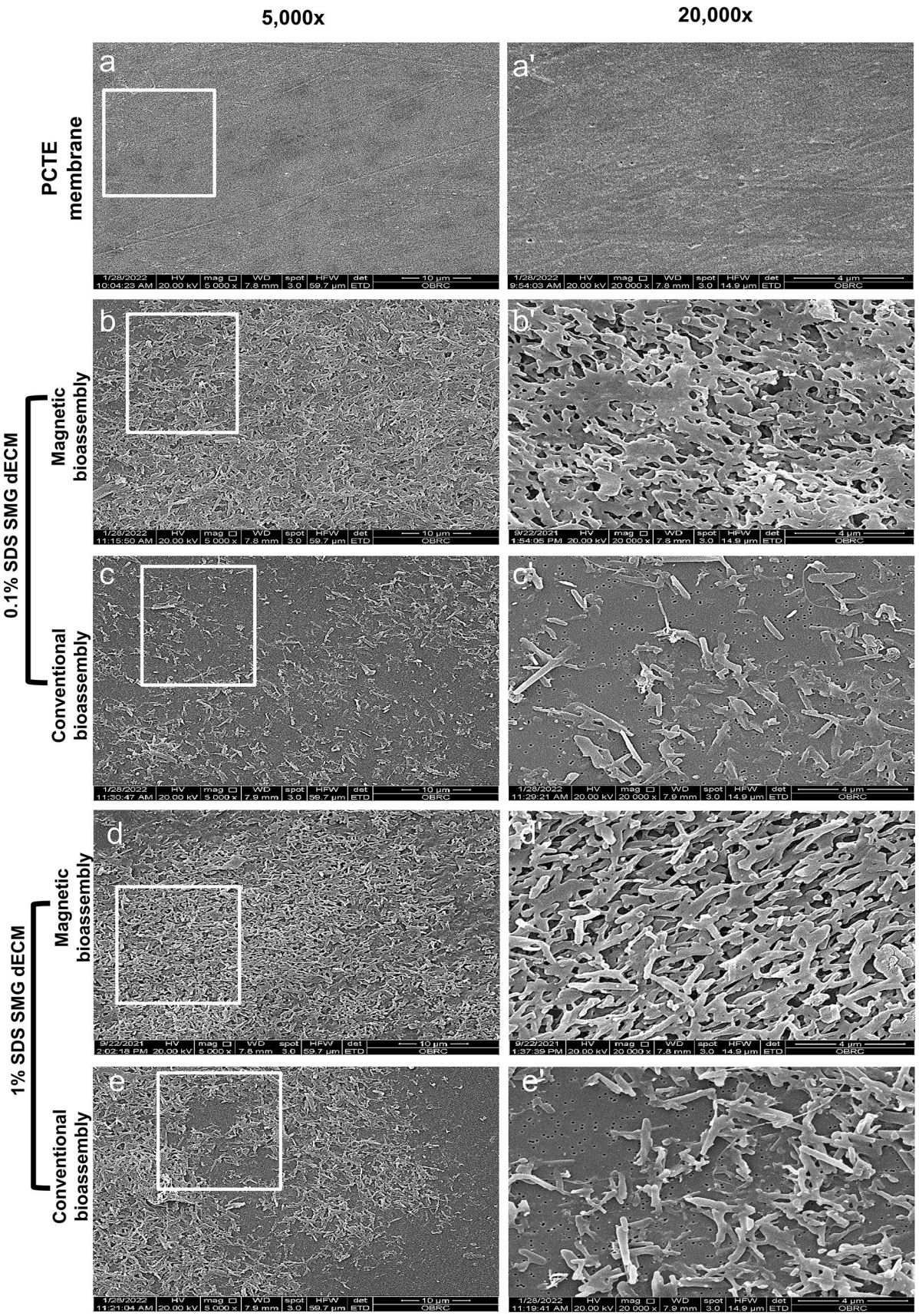
5,000x
20,000x
PCTE membrane
0.1% SDS SMG dECM
Magnetic bioassembly
Conventional bioassembly
1% SDS SMG dECM
Magnetic bioassembly
Conventional bioassembly
a
a'
b
b'
c
c'
d
d'
e
e'

◂**Fig. 4** Scanning electron microscopy was used to assess the ultrastructure of PCTE membrane, magnetic bio-assembled dECM, spin coating bio-assembled dECM (non-magnetic) of dECM perfused with 0.1% and 1% SDS treatments. A 10-fold rise in the SDS concentration increased the fine fibrillar threading of the retained biochemicals: inset images from white frames at 20,000 × magnifications. Scale bars: 10 µm and 4 µm (from left to right micrograph columns, respectively)

magnetic bio-assembled dECM platform exhibited consistency of our dECM platform and reproducibility towards cell viability, proliferation, and tethering. However, if a dECM amenable to easy handling and transfer to culture plates is an objective, in the long run, this SMG dECM biomaterial may need tunable matrix stiffness properties with the addition of a hydrogel component (Shin et al. 2019). These dECM

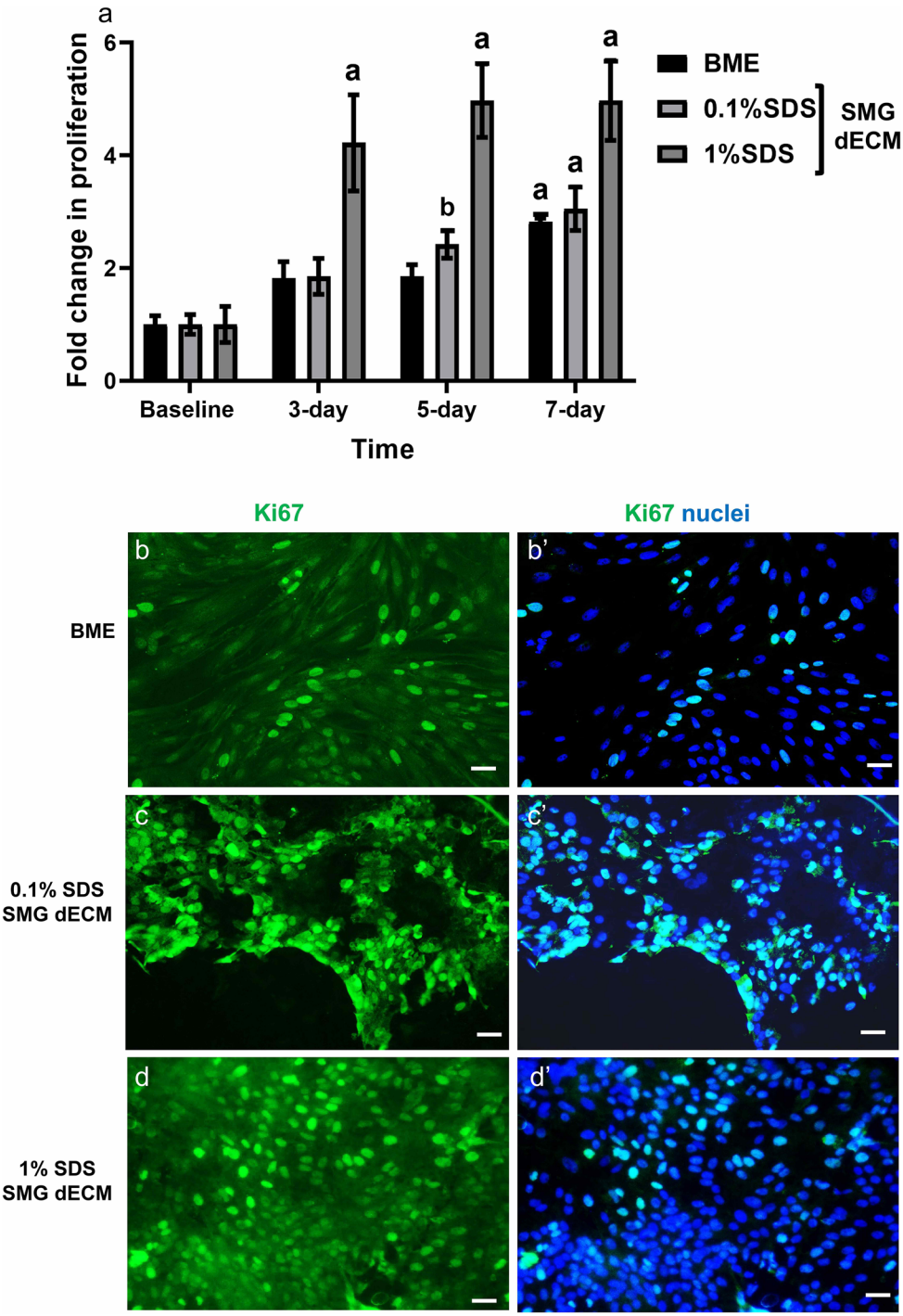

Fig. 5 Decellularized ECM magnetic-based bioassembly platforms supported primary SMG cell viability and proliferation. SMG dECM treated with 0.1% and 1% SDS were compared with commercial BME (basement membrane extract from Cultrex®). **a** Cell proliferation was assessed using the MTT assay, and fold change was determined by normalizing to baseline. Column bars represent means and error bars SD for $n = 4$ where a $p < 0.0001$ and b $p < 0.001$ relative to baseline in one-way ANOVA with Tukey post-hoc test. **b—d'** Expression of Ki67 was measured by immunoassaying. Mag.: 20 × Scale bar: 50 µm

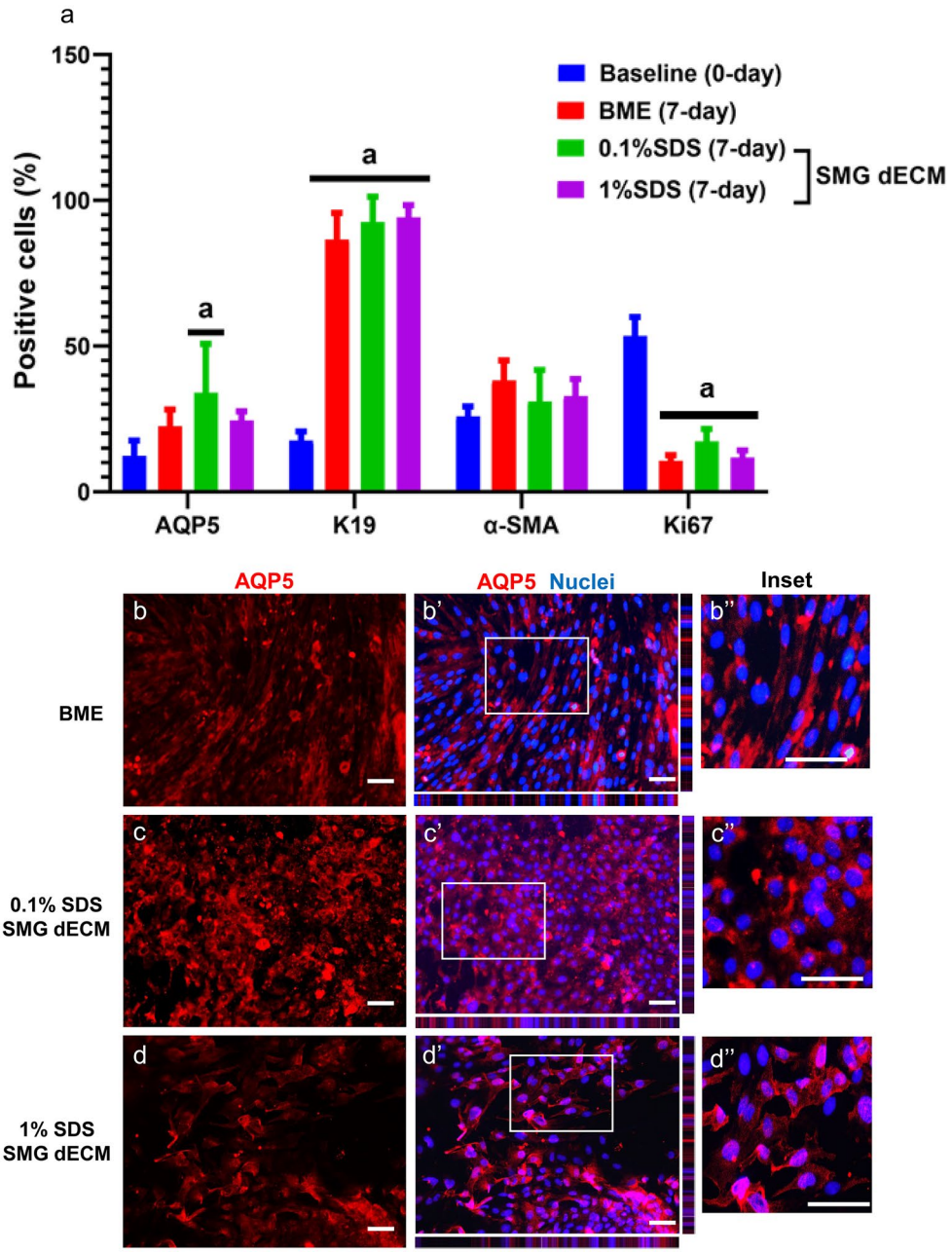

Fig. 6 Expression of epithelial differentiated and pro-mitotic markers in decellularized ECM magnetic bioassembly substrates. **a** The following commercial and bio-assembled substrates were used to assess protein expression: BME, SMG dECM treated with 0.1% and 1% SDS. Protein expression was determined via immunostaining by comparing fluorescence intensity of epithelial acinar (AQP5), ductal (K19), and myoepithelial (a-SMA) markers at day 7 relative to baseline (day 0) after normalizing to nuclear expression (DNA was stained with Hoechst 33,342). Ki67 marker was used to identify pro-mitotic cells. Error bars display SD for $n=6$ where a: $p<0.0001$ in comparison to either the baseline and/or other experimental groups with two-way ANOVA. **b–d''** Fluorescence micrographs of AQP5 expression observed after immunostaining and nuclear counterstain (Hoechst 33,342). **b–d'** Micrographs from left and center are at 20× magnification (scale bar: 50 µm). ImageJ-generated XYZ orthogonal projections are displayed next to the center merged micrographs. **b''–d''** Insets are a zoomed-in area from a white-framed region of interest in the center merged micrographs (40× magnification, scale bar: 20 µm)

biophysical properties are relevant for cancer organoid biofabrication platforms in mammary glands (i.e., breast cancer) and other epithelial organs like the lungs (Stowers et al. 2015; Nowak et al. 2017; Nerger and Nelson 2019; Liu et al. 2021; Berger et al. 2020), but these have not yet been fully investigated in SG morphogenesis (Patel et al. 2017, 2021). Nevertheless, these limitations can be overcome by adding magnetic nanoparticles to the dECM for tuning such biophysical properties. Nonetheless, conventional BME substrates and microbubble technologies also lack these tunable properties for SG organoid or microchip biofabrication (Hosseini et al. 2018; Song et al. 2021). Herein, tuning the SDS concentrations allowed for acinar or acinar plus ductal differentiation and different proliferation outputs. For instance, magnetic bioassembly substrates perfused with 0.1% SDS augmented both acinar and ductal epithelial cell populations (Fig. 6a, b), whereas 1% SDS supported only ductal differentiation and significantly increased cell proliferation rates at early culture (from day 3 onwards). Similar to conventional BME, all magnetic bioassembly substrates supported ductal epithelial differentiation (Fig. 6a; Supplementary Fig. 7). It has been demonstrated that dECM can support AQP5 expression and other tissue-specific cell phenotypes (Crabbé et al. 2015).

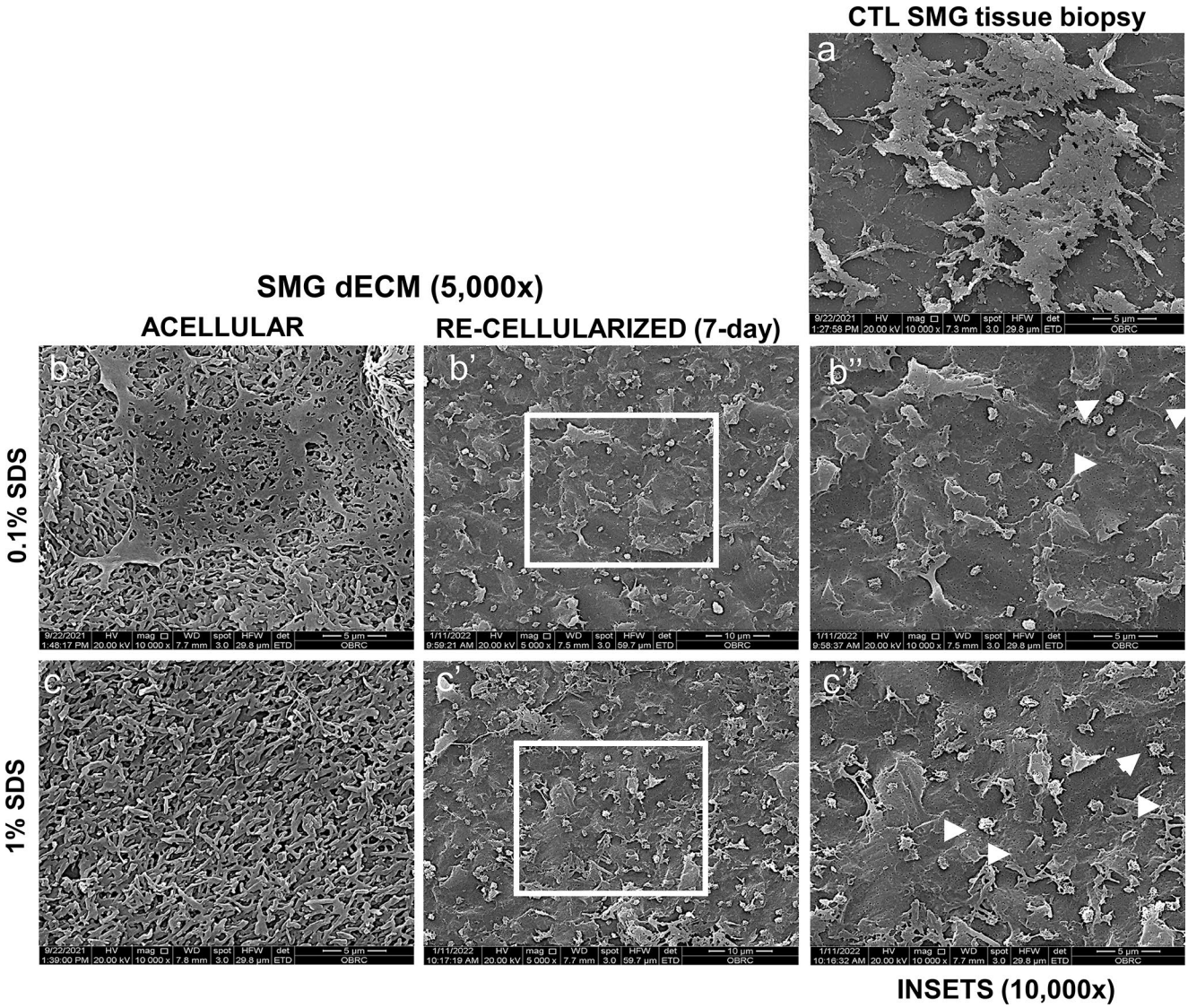

Fig. 7 Scanning electron micrographs of SMG dECM (magnetic bioassembly substrates) before and after recellularization after 7 culture days displayed higher tethering and recellularization with primary SMG cells in dECM perfused with 1% SDS. White arrowheads showed tethering of primary SMG cells on the SMG dECM. Right and left column micrographs are displayed at a mag. of 10,000×. Scale bar 5 µm and the middle micrographs are displayed at a mag. of 5000×. Scale bar 10 µm

Taken together, our newly developed strategy to decellularize human-mimicking ECM requires perfusions of 0.1–1% SDS to efficiently remove dsDNA/nuclear contents and maintain the mucins/sGAG biochemical niche and can potentially be tested in other exocrine gland tissues such as lacrimal gland, prostate, and exocrine pancreas. Biocompatibility properties such as proliferation and tethering of primary SMG cells onto the dECM confirmed that our dECM magnetic bioassembly platform can be explored in high throughput drug screening applications for healthy and cancer SG organoids. These novel dECM platforms can eventually support different cell types including human SG cancer cells, neural crest-derived adult stem cells, and genetically modified immortalized cells, although such in vitro investigations are still ongoing. Future steps towards the creation of a dECM bioink can also be taken by incorporating gelation and bioprintability processes into the finished SMG dECM product. The development of shear-thin hydrogels for 3D bioprinting can presumably be accomplished by combining the dECM with tunable hydrogels. For an accurate and exact deposition of the dECM bioink with an in-house extrusion-based printing platform, one must take into account other complex spatial and temporal aspects for appropriate bioprintability.

Supplementary Information The online version contains supplementary material available at https://doi.org/10.1007/s00441-022-03728-4.

Acknowledgements The authors are also grateful to Mr. Somchai Yodsanga from the Department of Oral Pathology, Faculty of Dentistry, Chulalongkorn University for providing support for the histological work and training for histology.

Funding This project was supported by the National Research Council of Thailand (NRCT) (grant number NRCT5-RSA63001-12) to J.N.F. and by the Faculty Research Grant (grant number DRF65001) from Faculty of Dentistry at Chulalongkorn University provided to J.N.F. Avatar Biotechnologies for Oral Health and Healthy Longevity Research Unit is funded by the Ratchadaphiseksomphot Endowment Fund, Chulalongkorn University. This research work was also supported by a postdoctoral scholarship grant to K.A. from The Second Century Fund (C2F), Chulalongkorn University. T.R. is funded by a Postdoctoral Fellowship from Ratchadapisek Somphot Fund, Chulalongkorn University.

Data availability Research data is available upon reasonable request to the corresponding author. Specific information related to the dECM methodology may not be disclosed due to pending patents.

Declarations

Ethics approval All applicable international, national, and institutional guidelines for the care and use of animals were followed accordingly. All experimental procedures were approved and conducted in accordance with the Chulalongkorn University Laboratory Animal Center (IACUC protocol number 1973004) and the Institutional Biosafety Committee at the Faculty of Dentistry Chulalongkorn University (DENT CU-IBC 027/2020 and DENT CU-IBC 026/2021).

Conflict of interest The authors declare no competing interests.

References

Adine C, Ng KK, Rungarunlert S, Souza GR, Ferreira JN (2018) Engineering innervated secretory epithelial organoids by magnetic three-dimensional bioprinting for stimulating epithelial growth in salivary glands. Biomaterials 180:52–66

Agarwal T, Narayan R, Maji S, Ghosh SK, Maiti TK (2018) Decellularized caprine liver extracellular matrix as a 2D substrate coating and 3D hydrogel platform for vascularized liver tissue engineering. J Tissue Eng Regen Med 12:e1678–e1690

Agostini BA, Cericato GO, da Silveira ER, Nascimento GG, Costa FDS, Thomson WM, Demarco FF (2018) How common is dry mouth? Systematic review and meta-regression analysis of prevalence estimates. Braz Dent J 29:606–618

Aisenbrey EA, Murphy WL (2020) Synthetic alternatives to Matrigel. Nat Rev Mater 5:539–551

Baptista PM, Siddiqui MM, Lozier G, Rodriguez SR, Atala A, Soker S (2011) The use of whole organ decellularization for the generation of a vascularized liver organoid. Hepatology 53:604–617

Berger AJ, Renner CM, Hale I, Yang X, Ponik SM, Weisman PS, Masters KS, Kreeger PK (2020) Scaffold stiffness influences breast cancer cell invasion via EGFR-linked Mena upregulation and matrix remodeling. Matrix Biol 85–86:80–93

Carlsson R, Engvall E, Freeman A, Ruoslahti E (1981) Laminin and fibronectin in cell adhesion: enhanced adhesion of cells from regenerating liver to laminin. Proc Natl Acad Sci USA 78:2403–2406

Carvalho SB, Moreira AS, Gomes J, Carrondo MJT, Thornton DJ, Alves PM, Costa J, Peixoto C (2018) A detection and quantification label-free tool to speed up downstream processing of model mucins. PLoS ONE 13:e0190974

Casali DM, Handleton RM, Shazly T, Matthews MA (2018) A novel supercritical CO2-based decellularization method for maintaining scaffold hydration and mechanical properties. J Supercrit Fluids 131:72–81

Chansaenroj A, Yodmuang S, Ferreira JN (2021) Trends in salivary gland tissue engineering: from stem cells to secretome and organoid bioprinting. Tissue Eng B Rev 27:155–165

Chen RN, Ho HO, Tsai YT, Sheu MT (2004) Process development of an acellular dermal matrix (ADM) for biomedical applications. Biomaterials 25:2679–2686

Choi HJ, Choi D (2013) Successful mouse hepatocyte culture with sandwich collagen gel formation. J Korean Surg Soc 84:202–208

Choi YC, Choi JS, Kim BS, Kim JD, Yoon HI, Cho YW (2012) Decellularized extracellular matrix derived from porcine adipose tissue as a xenogeneic biomaterial for tissue engineering. Tissue Eng Part C Methods 18:866–876

Chung JJ, Im H, Kim SH, Park JW, Jung Y (2020) Toward biomimetic scaffolds for tissue engineering: 3d printing techniques in regenerative medicine. Front Bioeng Biotechnol 8:1–12

Clara RLO, Robert AHV, Patrick WBD (2018) Re-inforcing the cell death army in the fight against breast cancer. J Cell Sci 131:212563

Crabbé ALY, Sarker SF, Bonenfant NR, Barrila J, Borg ZD, Lee JJ, Weiss DJ, Nickerson CA (2015) Recellularization of decellularized lung scaffolds is enhanced by dynamic suspension culture. PLoS ONE 5:e0126846

Crapo PM, Gilbert TW, Badylak SF (2011) An overview of tissue and whole organ decellularization processes. Biomaterials 32:3233–3243

Edmondson R, Broglie JJ, Adcock AF, Yang L (2014) Three-dimensional cell culture systems and their applications in drug discovery and cell-based biosensors. Assay Drug Dev Technol 12:207–218

Elebring E, Kuna VK, Kvarnström N, Sumitran-Holgersson S (2017) Cold-perfusion decellularization of whole-organ porcine pancreas supports human fetal pancreatic cell attachment and expression of endocrine and exocrine markers. J Tissue Eng 8:1–10

Fernández-Pérez J, Ahearne M (2019) The impact of decellularization methods on extracellular matrix derived hydrogels. Sci Rep 9

Ferraiolo DM, Veitz-Keenan A (2018) Insufficient evidence for interventions to prevent dry mouth and salivary gland dysfunction post head and neck radiotherapy. Evid Based Dent 1:30–31

Ferreira JN, Hasan R, Urkasemsin G, Ng KK, Adine C, Muthumariappan S, Souza GR (2019) A magnetic three-dimensional levitated primary cell culture system for the development of secretory salivary gland-like organoids. J Tissue Eng Regen Med 13:495–508

Ferreira LP, Gaspar VM, Mendes L, Duarte IF, Mano JF (2021) Organotypic 3D decellularized matrix tumor spheroids for high-throughput drug screening. Biomaterials 1:120983

Findeisen K, Morticelli L, Goecke T, Kolbeck L, Ramm R, Höffler HK, Brandes G, Korossis S, Haverich A, Hilfiker A (2020) Toward acellular xenogeneic heart valve prostheses: histological and biomechanical characterization of decellularized and enzymatically deglycosylated porcine pulmonary heart valve matrices. Xenotransplantation 27:1–19

Frantz C, Stewart KM, Weaver VM (2010) The extracellular matrix at a glance. J Cell Sci 123:4195–4200

Furness S, Bryan G, McMillan R, Worthington HV (2013) Interventions for the management of dry mouth: non-pharmacological interventions. Cochrane Database Syst Rev 30:CD009603

Gao Z, Wu T, Xu J, Liu G, Xie Y, Zhang C, Wang J, Wang S (2015) Generation of bioartificial salivary gland using whole-organ decellularized bioscaffold. Cells Tissues Organs 200:171–180

Gilpin A, Yang Y (2017) Decellularization strategies for regenerative medicine: from processing techniques to applications. Biomed Res Int 2017:9831534

Gilpin SE, Guyette JP, Gonzalez G, Ren X, Asara JM, Mathisen DJ, Vacanti JP, Ott HC (2014) Perfusion decellularization of human and porcine lungs: bringing the matrix to clinical scale. J Heart Lung Transplant 33:298–308

Gil-Ramírez A, Rosmark O, Spégel P, Swärd K, Westergren-Thorsson G, Larsson-Callerfelt AK, Rodríguez-Meizoso I (2020) Pressurized carbon dioxide as a potential tool for decellularization of pulmonary arteries for transplant purposes. Sci Rep 10:1–12

Giobbe GG, Crowley C, Luni C, Campinoti S, Khedr M, Kretzschmar K, De Santis MM, Zambaiti E, Michielin F, Meran L, Hu Q, van Son G, Urbani L, Manfredi A, Giomo M, Eaton S, Cacchiarelli D, Li VSW, Clevers H, Bonfanti P, Elvassore N, De Coppi P (2019) Extracellular matrix hydrogel derived from decellularized tissues enables endodermal organoid culture. Nat Commun 10:5658

Hashemi J, Pasalar P, Soleimani M, Arefian E, Khorramirouz R, Akbarzadeh A, Ghorbani F, Enderami SE, Kajbafzadeh AM (2018) Decellularized pancreas matrix scaffolds for tissue engineering using ductal or arterial catheterization. Cells Tissues Organs 205:72–84

Hashimoto Y, Hattori S, Sasaki S, Honda T, Kimura T, Funamoto S, Kobayashi H, Kishida A (2016) Ultrastructural analysis of the decellularized cornea after interlamellar keratoplasty and microkeratome-assisted anterior lamellar keratoplasty in a rabbit model. Sci Rep 6:1–9

Haupt J, Lutter G, Gorb SN, Simionescu DT, Frank D, Seiler J, Paur A, Haben I (2018) Detergent-based decellularization strategy preserves macro- a nd microstructure of heart valves. Interact Cardiovasc Thorac Surg 26:230–236

Hosseini ZF, Nelson DA, Moskwa N, Sfakis LM, Castracane J, Larsen M (2018) FGF2-dependent mesenchyme and laminin-111 are niche factors in salivary gland organoids. J Cell Sci 131:jcs208728

Jorgensen M, Ramesh P, Toro M, Evans E, Moskwa N, Zhang X, Sharfstein ST, Larsen M, Xie Y (2022) Alginate hydrogel microtubes for salivary gland cell organization and cavitation. Bioengineering 9(1):38

Kaur S, Kaur I, Rawal P, Tripathi DM, Vasudevan A (2021) Non-matrigel scaffolds for organoid cultures. Cancer Lett 504:58–66

Kim I, Yang DJ, Donnelly DF, Carroll JL (2009) Fluoresceinated peanut agglutinin (PNA) is a marker for live O(2) sensing glomus cells in rat carotid body. Adv Exp Med Biol 648:185–190

Lee JS, Shin J, Park HM, Kim YG, Kim BG, Oh JW, Cho SW (2014) Liver extracellular matrix providing dual functions of two-dimensional substrate coating and three-dimensional injectable hydrogel platform for liver tissue engineering. Biomacromol 15:206–218

Lee SW, Kim J, Do M, Namkoong E, Lee H, Ryu JH, Park K (2020) Developmental role of hyaluronic acid and its application in salivary gland tissue engineering. Acta Biomater 115:275–287

Li J, Cai Z, Cheng J, Wang C, Fang Z, Xiao Y, Feng ZG, Gu Y (2020) Characterization of a heparinized decellularized scaffold and its effects on mechanical and structural properties. J Biomater Sci Polym Ed 31:999–1023

Lin H, Sun G, He H, Botsford B, Li M, Elisseeff JH, Yiu SC (2016) Three-dimensional culture of functional adult rabbit lacrimal gland epithelial cells on decellularized scaffold. Tissue Eng Part A 22(1–2):65–74

Lin HJ, Wang TJ, Li TW, Chang YY, Sheu MT, Huang YY, Liu DZ (2019) Development of decellularized cornea by organic acid treatment for corneal regeneration. Tissue Eng Part A 25:652–662

Liu C, Li M, Dong ZX, Jiang D, Li X, Lin S, Chen D, Zou X, Zhang XD, Luker GD (2021) Heterogeneous microenvironmental stiffness regulates pro-metastatic functions of breast cancer cells. Acta Biomater 131:326–340

Mabrouk M, Beherei HH, Das DB (2020) Recent progress in the fabrication techniques of 3D scaffolds for tissue engineering. Mater Sci Eng C 110:110716–110716

Maria OM, Maria O, Liu Y, Komarova SV, Tran SD (2011) Matrigel improves functional properties of human submandibular salivary gland cell line. Int J Biochem Cell Biol 43:622–631

Mayorca-Guiliani AE, Willacy O, Madsen CD, Rafaeva M, Elisabeth Heumüller S, Bock F, Sengle G, Koch M, Imhof T, Zaucke F, Wagener R, Sasaki T, Erler JT, Reuten R (2019) Decellularization and antibody staining of mouse tissues to map native extracellular matrix structures in 3D. Nat Protoc 14:3395–3425

Mercadante V, Al Hamad A, Lodi G, Porter S, Fedele S (2017) Interventions for the management of radiotherapy-induced xerostomia and hyposalivation: a systematic review and meta-analysis. Oral Oncol 66:64–74

Miranda-Rius J, Brunet-Llobet L, Lahor-Soler E, Farré M (2015) Salivary secretory disorders, inducing drugs, and clinical management. Int J Med Sci 12:811–824

Nam K, Maruyama CL, Wang CS, Trump BG, Lei P, Andreadis ST, Baker OJ (2017) Laminin-111-derived peptide conjugated fibrin hydrogel restores salivary gland function. PLoS ONE 12:e0187069

Nerger BA, Nelson CM (2019) 3D culture models for studying branching morphogenesis in the mammary gland and mammalian lung. Biomaterials 198:135–145

Nie J, Gao Q, Fu J, He Y (2020) Grafting of 3D bioprinting to in vitro drug screening: a review. Adv Healthcare Mater 9:1901773

Nowak M, Freudenberg U, Tsurkan MV, Werner C, Levental KR (2017) Modular GAG-matrices to promote mammary epithelial morphogenesis in vitro. Biomaterials 112:20–30

Patel VN, Pineda DL, Berenstein E, Hauser BR, Choi S, Prochazkova M, Zheng C, Goldsmith CM, van Kuppevelt TH, Kulkarni A, Song Y, Linhardt RJ, Chibly AM, Hoffman MP (2021) Loss of Hs3st3a1 or Hs3st3b1 enzymes alters heparan sulfate to reduce epithelial morphogenesis and adult salivary gland function. Matrix Biol 103–104:37–57

Patel VN, Pineda DL, Hoffman MP (2017) The function of heparan sulfate during branching morphogenesis. Matrix Biol 57–58:311–323

Petrou G, Crouzier T (2018) Mucins as multifunctional building blocks of biomaterials. Biomater Sci 6:2282–2297

Poornejad N, Schaumann LB, Buckmiller EM, Momtahan N, Gassman JR, Ma HH, Roeder BL, Reynolds PR, Cook AD (2016) The impact of decellularization agents on renal tissue extracellular matrix. J Biomater Appl 31:521–533

Pringle S, Nanduri LS, van der Zwaag M, van Os R, Coppes RP (2011) Isolation of mouse salivary gland stem cells. J Vis Exp (48):2484. https://doi.org/10.3791/2484

Ramm R, Goecke T, Theodoridis K, Hoeffler K, Sarikouch S, Findeisen K, Ciubotaru A, Cebotari S, Tudorache I, Haverich A, Hilfiker A (2020) Decellularization combined with enzymatic removal of N-linked glycans and residual DNA reduces inflammatory response and improves performance of porcine xenogeneic pulmonary heart valves in an ovine in vivo model. Xenotransplantation 27:1–12

Rijal G, Wang J, Yu I, Gang DR, Chen RK, Li W (2018) Porcine breast extracellular matrix hydrogel for spatial tissue culture. Int J Mol Sci 19:2912

Riley P, Glenny AM, Hua F, Worthington HV (2017) Pharmacological interventions for preventing dry mouth and salivary gland dysfunction following radiotherapy. Cochrane Database Systematic Reviews 31:CD012744

Rodboon T, Yodmuang S, Chaisuparat R, Ferreira JN (2021) Development of high-throughput lacrimal gland organoid platforms for drug discovery in dry eye disease. SLAS Discovery S2472–5552(21):00017–00024

Santoso EG, Yoshida K, Hirota Y, Aizawa M, Yoshino O, Kishida A, Osuga Y, Saito S, Ushida T, Furukawa KS (2014) Application of detergents or high hydrostatic pressure as decellularization processes in uterine tissues and their subsequent effects on in vivo uterine regeneration in murine models. PLoS ONE 9:e103201

Shin K, Koo KH, Jeong J, Park SJ, Choi DJ, Ko YG, Kwon H (2019) Three-dimensional culture of salivary gland stem cell in orthotropic decellularized extracellular matrix hydrogels. Tissue Eng Part A 25:1396–1403

Song Y, Uchida H, Sharipol A, Piraino L, Mereness JA, Ingalls MH, Rebhahn J, Newlands SD, DeLouise LA, Ovitt CE, Benoit DSW (2021) Development of a functional salivary gland tissue chip with potential for high-content drug screening. Commun Biol 19:361

Stapleton TW, Ingram J, Katta J, Knight R, Korossis S, Fisher J, Ingham E (2008) Development and characterization of an acellular porcine medial meniscus for use in tissue engineering. Tissue Eng Part A 14:505–518

Stowers RS, Allen SC, Suggs LJ (2015) Dynamic phototuning of 3D hydrogel stiffness. Proc Natl Acad Sci USA 112:1953–1958

Sui Y, Zhang S, Li Y, Zhang X, Hu W, Feng Y, Xiong J, Zhang Y, Wei S (2020) Generation of functional salivary gland tissue from human submandibular gland stem/progenitor cells. Stem Cell Res Ther 11:1–13

Tanaka J, Mishima K (2020) In vitro three-dimensional culture systems of salivary glands. Pathol Int 70:493–501

Tanaka J, Mishima K (2021) Application of regenerative medicine to salivary gland hypofunction. Jpn Dent Sci Rev 57:54–59

Truong TM, Nguyen VM, Tran TT, Le TM (2021) Characterization of acid-soluble collagen from food processing by-products of snakehead fish (Channa striata). Processes 9:1188

Uhl FE, Zhang F, Pouliot RA, Uriarte JJ, Rolandsson Enes S, Han X, Ouyang Y, Xia K, Westergren-Thorsson G, Malmström A, Hallgren O, Linhardt RJ, Weiss DJ (2020) Functional role of glycosaminoglycans in decellularized lung extracellular matrix. Acta Biomater 102:231–246

Urkasemsin G, Castillo P, Rungarunlert S, Klincumhom N, Ferreira JN (2019) Strategies for developing functional secretory epithelia from porcine salivary gland explant outgrowth culture models. Biomolecules 9(11):657. https://doi.org/10.3390/biom9110657

Wasnik S, Kantipudi S, Kirkland MA, Pande G (2016) Enhanced ex vivo expansion of human hematopoietic progenitors on native and spin coated acellular matrices prepared from bone marrow stromal cells. Stem Cells Int 2016:7231567. https://doi.org/10.1155/2016/7231567

White LJ, Taylor AJ, Faulk DM, Keane TJ, Saldin LT, Reing JE, Swinehart IT, Turner NJ, Ratner BD, Stephen F (2017) The impact of detergents on the tissue decellularization process: a ToF-SIMS study. Acta Biomater 50:207–219

Wolf MT, Daly KA, Brennan-Pierce EP, Johnson SA, Carruthers CA, D'Amore A, Nagarkar SP, Velankar SS, Badylak SF (2012) A hydrogel derived from decellularized dermal extracellular matrix. Biomaterials 33:7028–7038

Zang M, Zhang Q, Chang EI, Mathur AB, Yu P (2012) Decellularized tracheal matrix scaffold for tissue engineering. Plast Reconstr Surg 130:532–540